Hindawi
International Journal of RF and Microwave Computer-Aided Engineering
Volume 2024, Article ID 2555206, 19 pages
https://doi.org/10.1155/2024/2555206

Research Article

Implanted Rhombus Ring Partial Inset-Fed Circularly Polarized Microstrip Monopole Antenna for WBAN Applications

Mohamed Njianga Yende,[1] **Ghanshyam Singh**,[2] **Guy Ayissi Eyebe**,[1,3] **Clement Mbinack**,[1] **and Joseph Mebara Mbida**[1]

[1]*Laboratory of Electronics, Department of Physics, Faculty of Sciences, University of Yaounde I, Yaounde, Cameroon*
[2]*Department of Electronics and Communication Engineering, Feroze Gandhi Institute of Engineering and Technology, Reabareli 229316, India*
[3]*Department of Electrical and Computer Engineering, University of Quebec, Trois-Rivieres, Canada*

Correspondence should be addressed to Mohamed Njianga Yende; njiangayendemohamed@gmail.com

Received 20 April 2023; Revised 7 June 2023; Accepted 1 February 2024; Published 15 February 2024

Academic Editor: N. Nasimuddin

In the present article, a design approach to accomplish circular polarization-based rhombus ring microstrip-fed monopole antenna working at 5.8 GHz for wireless body area network (WBAN) applications is proposed. The input impedance calculation using an electromagnetic theory of transmission line in a travelling wave coupled to the parallel-plate inductor model is conducted. Radiated electric field pattern calculation of the conventional square ring microstrip patch antenna (MSPA) using Biot and Savart's law is reported. The circular polarization of the proposed antenna is accomplished by loading the radiating path with a capacitive element sectioned in the neighbourhood of the feed line. The proposed planar monopole antenna of volume $0.38\lambda_0 \times 0.38\lambda_0 \times 0.029\lambda_0$ (λ_0 is evaluated at the resonant frequency of 5.8 GHz) achieves a -10 dB impedance bandwidth of 86.20% in the band (3-8 GHz) with a stable real gain of 8.29 dBic in circular polarization at the resonant frequency of 5.8 GHz and axial ration bandwidth of about 32.75% in the (5-6.9 GHz) band. Specific absorption rate (SAR) evaluation of the studied antenna is computed numerically on a part of the human phantom model to justify its use in WBAN applications. It is noted that the maximum amount of radiation absorbed by a part of the human phantom model is limited to a maximum SAR value of 1.45 W/kg and 0.754 W/kg on 1 g and 10 g of tissue mass, respectively. The prospective design has been fabricated and tested, and the experimental results are in good agreement with the simulation outcomes.

1. Introduction

Wireless body area network (WBAN) is a communication technology using free space as the transmission channel, which consists of interconnecting in, on, or around the human body tiny devices that can perform measurements (sensors) or act actively (actuators) or in our case, the transmission of RF signals (body antennas) [1]. These devices, which are highly autonomous and use very low power currents, can be capable of communicating with a remote service centre, to alert a hospital emergency service for example [2]. The main applications are quite extensive, notably in various fields, both civil and military, such as survival and geolocation of soldiers on the battlefield, performance of athletes, health monitoring, and patient follow-up [3]. Indeed, these wireless transmission systems are increasingly used in medical applications outside the human body in medical diagnosis and therapeutic monitoring for various applications [4]. They are placed on the patient's clothing in order to transmit vital information (heartbeat per minute, blood pressure, and body temperature) and thus monitor the evolution of vital parameters [5].

During the last decade, several structure-based antennas have been developed such as vertical monopoles, microstrip monopoles [6], planar inverted F-antennas [7], microstrip patch antennas [8], waveguide-fed cavity, and planar slot antennas [9, 10] to achieve the requirement of the targeted application. Typically, microstrip patch antenna (MSPA)

Table 1: Previous works with their performance parameters.

References	Frequency (GHz)	Dimension (mm^3)	Impedance bandwidth (%)	3 dB ARBW (%)	Peak gain
[17]	4.74	$20 \times 20 \times 1.5$	36.9	9.98	3.0 dBic
[18]	5.8	$52 \times 52 \times 100$	19.82	11.1	11.1 dBic
[19]	4.5	$52 \times 52 \times 14$	15.0	11.0	6.2 dBi
[20]	2.23, 2.84, 3.19, 3.83	$35 \times 30 \times 1.6$	3.58, 2.64, 2.50, and 1.82	-1.41, 3.12, and 1.57	2.05, 1.3, 0.76, and 0.3 dB
[21]	2.48, 3.16	$35 \times 30 \times 1.6$	6.04 and 1.94	—	1.05 and 1.09 dB
[22]	23.9, 30.7	$19.76 \times 19.76 \times 0.51$	25	—	9.4 dBic
[23]	3.6	$28 \times 28 \times 1.6$	10.9	4.12	2.5 dB
[24]	3.45	$80 \times 80 \times 10.43$	30	—	9.9 dBi

use popularity increased, and many modern wireless communication systems based on MSPA have been developed specially for WBAN applications. However, they have exhibited at least one of the following problems: very narrow bandwidth, high profile, and high radiation to the body. In order to solve these different problems, several methods and techniques have been developed in the literature such as genetic algorithm [11], metamaterial technology [12, 13], graphene-based substrate [14], hammer-type antenna [15], and neural networks [16]. However, the disadvantage of these antennas is the difficulty of alignment between linearly polarized signals due to the characteristics of the external environment that disturb the polarization. To overcome these linear polarization constraints, solutions have been proposed: A low-profile circularly polarized (CP) microstrip antenna using an elliptical electromagnetic band gap structure was developed [17]. In [18], a 3-D printed circularly polarized (CP) open-ended waveguide antenna array based on an in-built antipodal exponential groove polarizer was investigated. In [19], a new dual circular polarized (CP) microstrip antenna fed by a dual L-shaped probe and emitting electromagnetic waves above and below the substrate was reported. A modified electric-inductive-capacitive resonator (m-ELC) and an arrow-shaped stub are introduced into the patch and ground plane of a quad-band multipolarized antenna with a truncated corner [20]. In [21], a compact patch antenna with truncated corners is loaded with complementary D-shaped split ring resonator (D-CSRR) structures at the ground plane, a compact MIMO antenna using a square ring resonator (SQRR) metasurface and a radiating patch [22]. A single-element circularly polarized (CP) MIMO microstrip antenna with two pairs of unequal slots was investigated [23]. A differential-fed, dual-polarized, broadband filtering microstrip antenna with high suppression and wide stopband was presented in [24]. The different characteristics of his previous work have been grouped in Table 1.

In this work, we propose the design of a circular polarized wideband 50 Ω microstrip-fed line split rhombus ring microstrip monopole antenna (SRRMMA) for WBAN applications. The proposed antenna is numerically tested on a part of the human phantom model. The antenna is developed on a solid dielectric substrate to overcome the problems associated with body antennas [25]. Circular

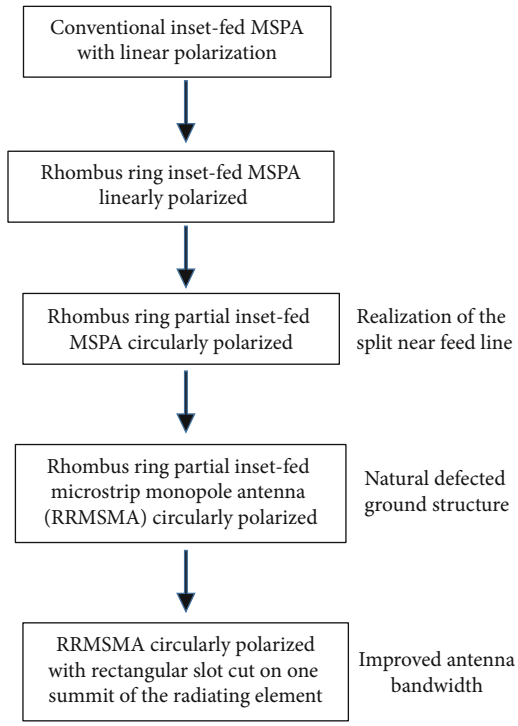

Figure 1: Flow chart of the proposed design approach of the studied antenna.

polarization is another important performance parameter of the body antenna to be considered because the movement and the position of the human phantom can disturb the polarization of the body-worn antenna. The input impedance and the radiated electric field at a far distance of the conventional square ring microstrip patch antenna (SRMSPA) are calculated analytically using an electromagnetic theory of transmission line in a travelling wave in conjunction with the parallel-plate inductor modelling the antenna and Biot and Savart's law approaches, respectively. The SRMSPA has been chosen to conduct output performance calculation because it was observed that the rhombus ring or square ring has the same radiation characteristics and the square ring model is simple to explain the radiation mechanism and the calculation hypothesis. Simulation results on CST-MWS software of the proposed antenna on

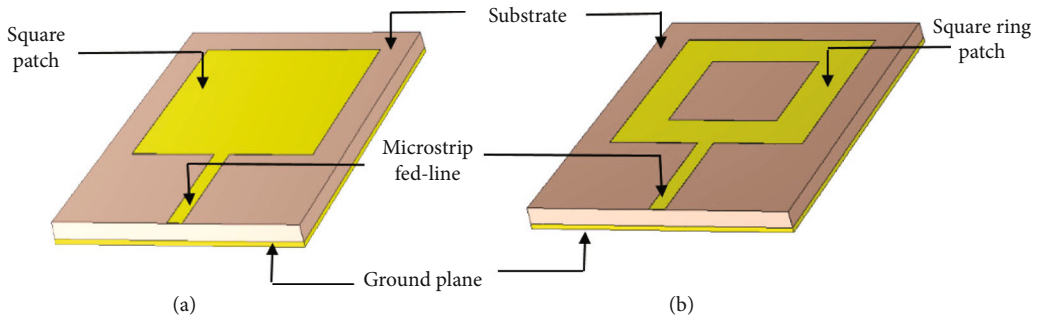

Figure 2: Geometry of the antenna studied. (a) Conventional microstrip patch antenna (MSPA). (b) Square ring microstrip patch antenna (SRMSPA).

a part of the phantom body in terms of input impedance, radiated pattern, -10 dB impedance bandwidth, 3 dB axial ratio, gain, and specific absorption rate (SAR) are analyzed and discussed. To describe the different steps of the design approach, the following flow chart is proposed in Figure 1.

2. Geometry of the Base Antenna

The geometry of the conventional MSPA and the SRMSPA fed by a 50 Ω-microstrip line is shown in Figure 2, and its overall dimension is $0.5\lambda_0 \times 0.5\lambda_0 \times 0.029\lambda_0$ (λ_0 is evaluated at the resonant frequency of 5.8 GHz) and is well explained in [26]. The geometry reported in Figure 2(b) is obtained from Figure 2(a) by cutting a part of the metallization of the square patch.

Figure 2(b) depicts a complete SRMSPA with the feed line, which is considered a regular geometry, and the current distribution due to the feed line follows two paths. These two current halves rotate in opposite directions, thus forcing the cancellation of the electromagnetic fields due to these currents. The actual structure maintains linear polarization that steads a limit to overcome for a moving subject (human in motion). To achieve circular polarization, some modifications must be applied to the radiating ring without degradation of its output performances.

3. Principal Modification

To obtain a circular polarization and the improvement of the axial ratio, the square ring (MSPA) is replaced by a rhombus ring (MSPA) and part of the ring is cut off near the feed line of dimensions $L_4 \times W_7$ (in mm^2). These modifications associated with DGS are the principal design approach to obtain the proposed split rhombus ring microstrip monopole antenna (SRRMSMA) as illustrated in Figure 3.

This modification transforms the RRMSMA from regular to irregular configuration by cutting a part of metallization at one side of the notch to obtain the SRRMSMA. The split of dimensions $L_4 \times W_7$ is illustrated in Figure 4 with all the optimized antenna parameters. Thus, the rotation of the right-hand current governs to support circular polarization with the irregular patch, and the axial ratio is reduced to below the value of 3 dB. The surface current distribution of

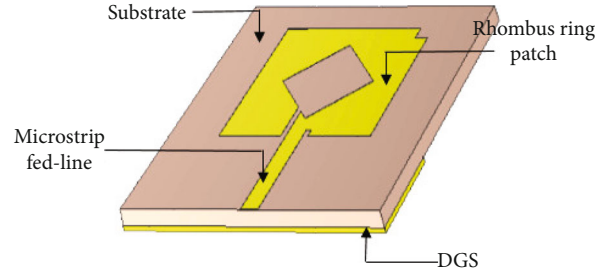

Figure 3: Structure of the proposed SRRMSA.

the irregular end geometry is observed at four different phases (0°, 90°, 180°, and 270°) for 5.8 GHz, as shown in Figure 5. The rotational current elements are circled on four phases to ensure the circular polarization for the proposed structure. In state-of-the-art, the DGS is responsible for the dual-band of the MSPA. However, it was noted that the rhombus ring microstrip monopole antenna (RRMSMA) does not generate a dual-band. Additionally, the split imposes a right current circulation according to the microstrip-fed line. Analysing the considered structure-based bore effects, at the level of the split, it appears two electric field components, one perpendicular to the metallization and the other parallel to the metallization. It is an electric field behavior that can explain circular polarization. Given that the circular polarization of the proposed antenna is important, the split width must also be as important as possible. This induces the necessity to optimize antenna parameters as depicted in Figure 4 and reported in Table 2.

In this design approach, the split is responsible for the circular polarization, whereas the square slot of dimensions $W_9 \times W_9$ cut on one vertex of the radiating element as demonstrated in Figure 4(a) is responsible for the improvement of the bandwidth. The front view and back view of the fabricated prototype are portrayed in Figures 6(a) and 6(b), respectively. An appropriate parametric optimization is carried out to have the resonant frequency well below the -10 dB value of the reflection coefficient so that the proposed geometry can be suitably used in wireless communication systems where wide bandwidth is the demand.

The antenna is planar low profile, has a single port, is very easy to design, is fabricated, and is also efficient. Sensors

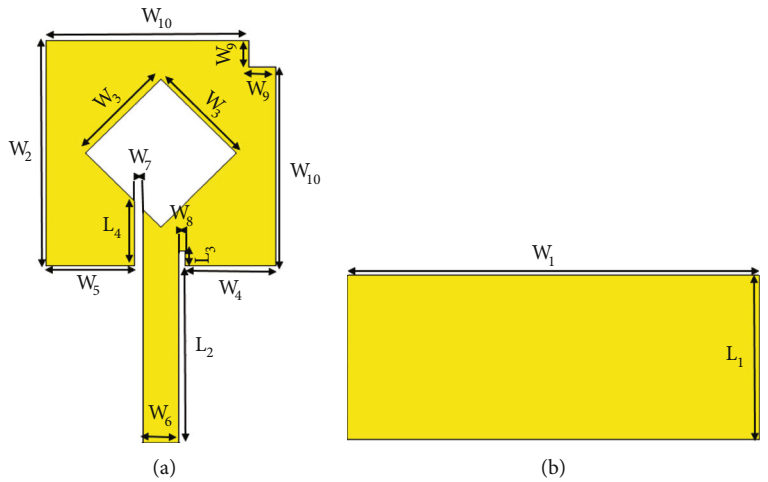

FIGURE 4: Dimensions of the proposed antenna. (a) Front view. (b) Back view.

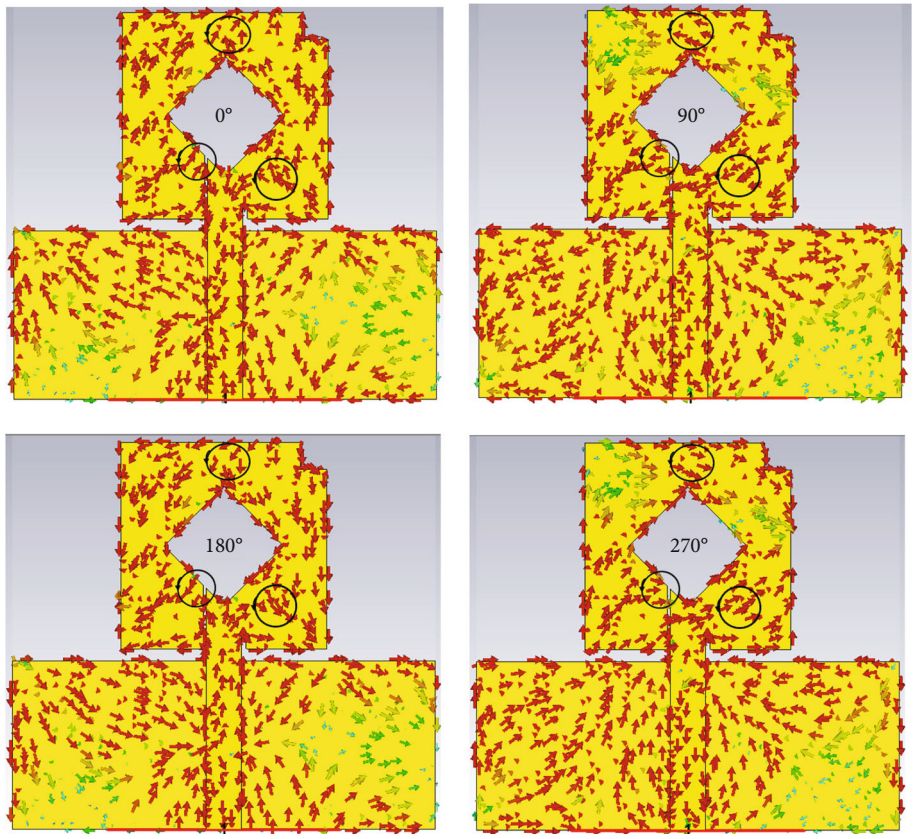

FIGURE 5: Surface current distributions over the proposed geometry at 5.8 GHz for four different excitation phases.

TABLE 2: Optimized parameter values of the proposed rhombus ring antenna.

Parameter	W_1	W_2	W_3	W_4	W_5	W_6	W_7	W_8	W_9	W_{10}	L_1	L_2	L_3	L_4
Value (in mm)	40	19.5	8	8.169	8.269	3.362	0.3	0.4	2.5	17	15.92	17	1.45	10

working as implanted biomedical wireless systems can be equipped with this antenna as on body antenna to communicate with access points around the human body via a 5.8 GHz off-body antenna hand and send received information to the remote service centre via 5.2/5.8 WLAN band for rapid patient care.

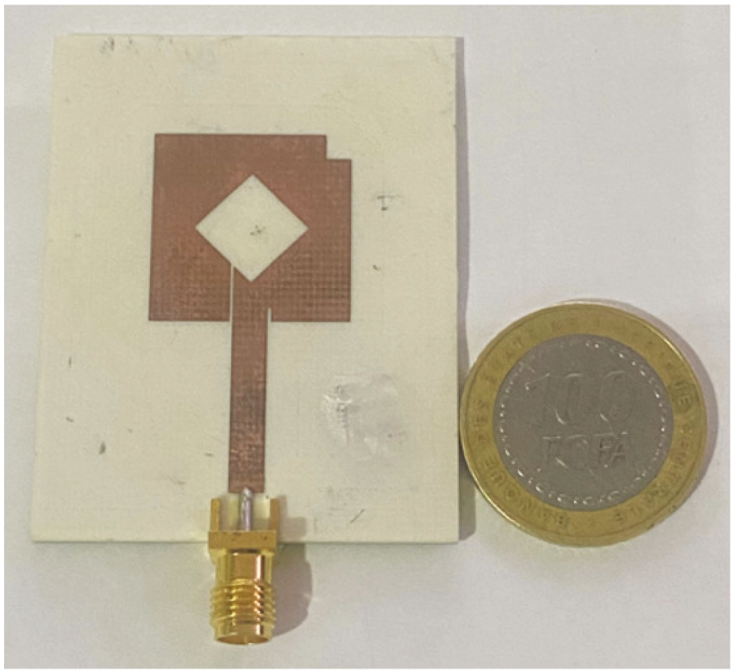

(a)

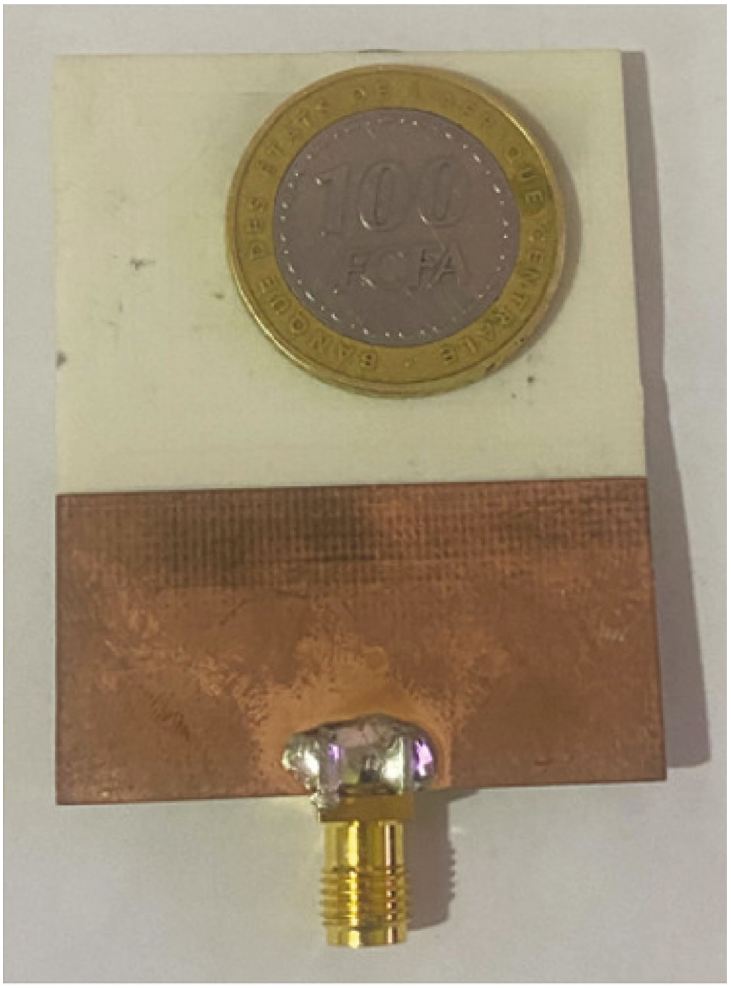

(b)

Figure 6: Photograph of the fabricated antenna. (a) Front view. (b) Back view.

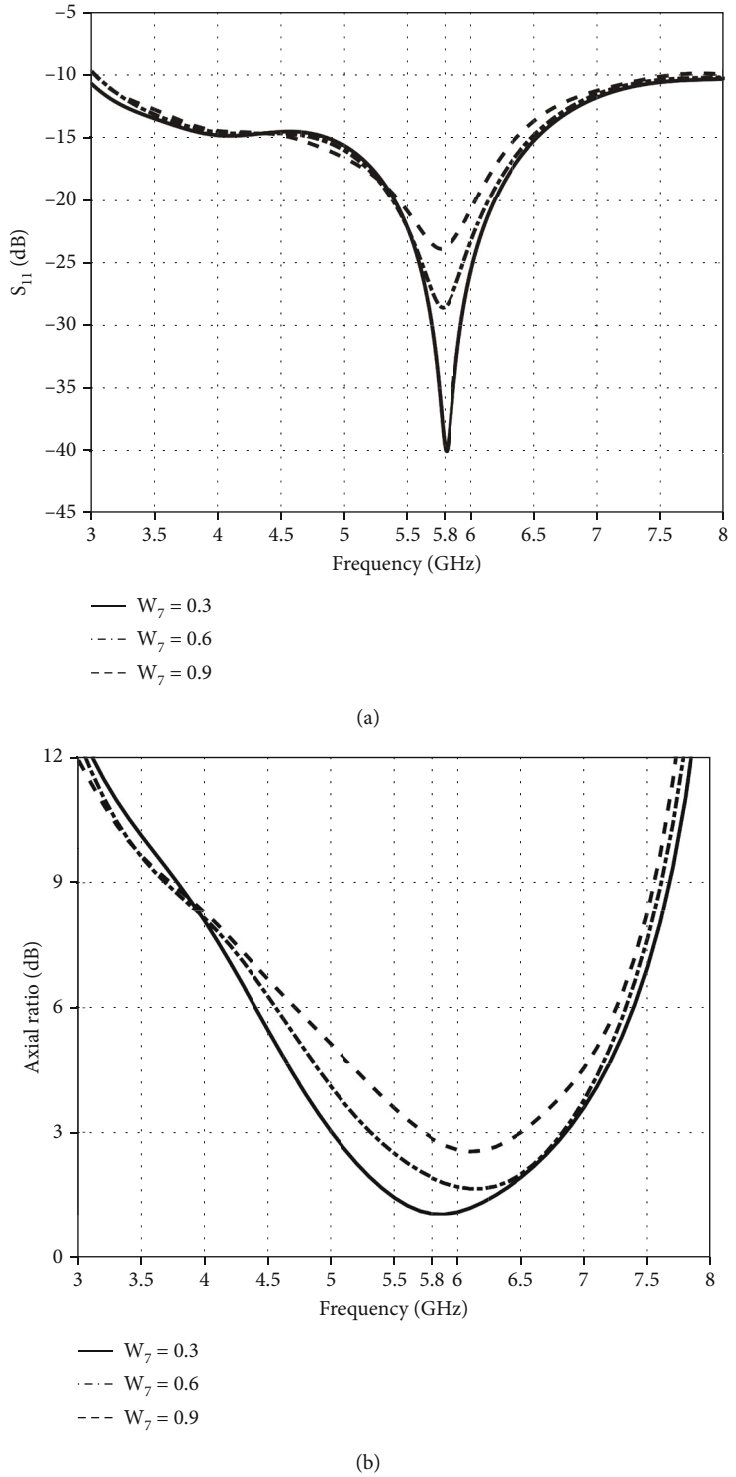

FIGURE 7: Influence of slot width (W_7) on (a) S_{11} parameter and (b) axial ratio.

4. Parametric Investigation

In this section, parametric analyses of the proposed antenna are shown by varying outer ring (W_2), inner ring (W_3), the slot (W_7), and the square slot (W_9) to see their influence on the performance of the structure, especially in terms of matching over a frequency bandwidth and also on the axial ratio. Figures 7–10 show the parametric study of W_7, W_3, W_2, and W_9, respectively.

4.1. The Influence of the Parameter W_7 on the Bandwidth and the Axial Ratio. Figure 7 shows that the axial ratio bandwidth is maximum for $W_7 = 0.3$ mm. Therefore, W_7 is a very

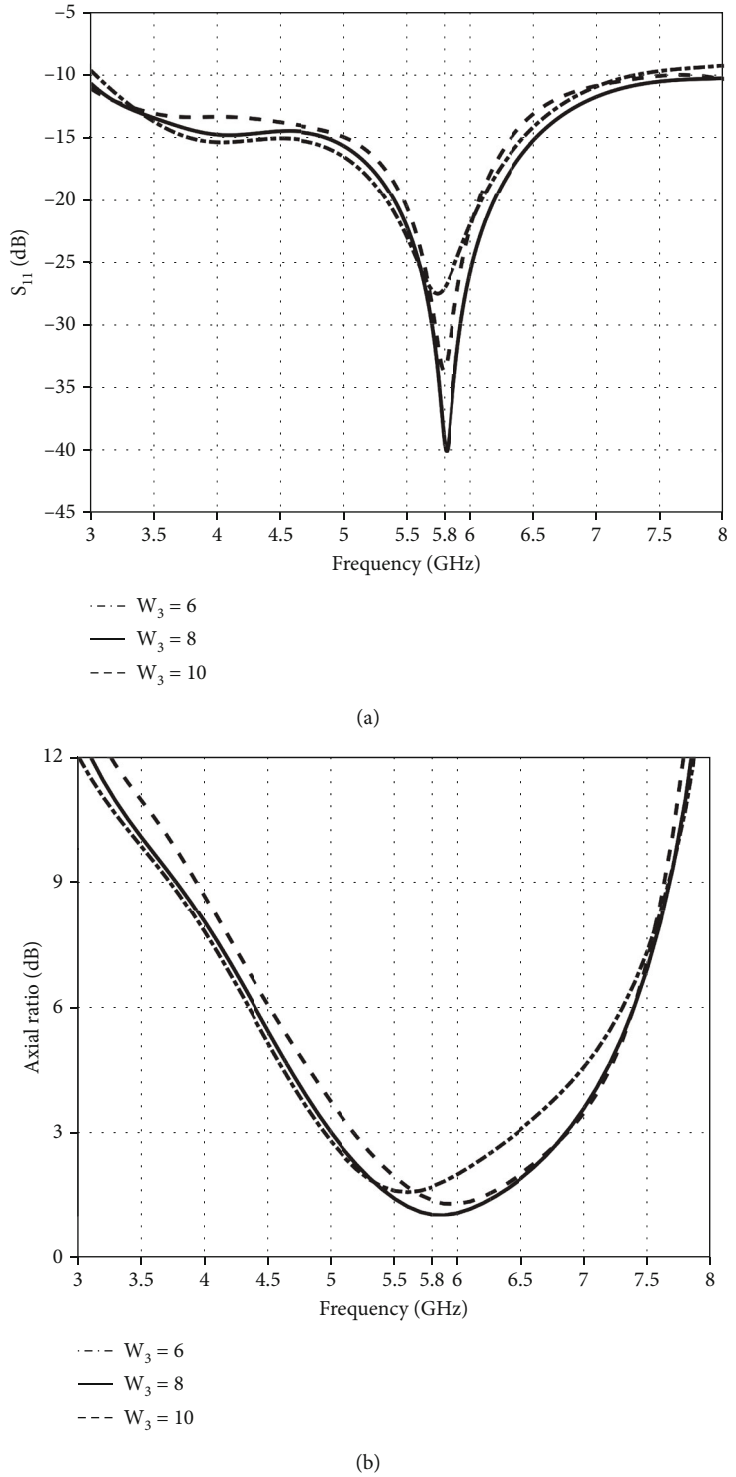

FIGURE 8: Influence of slot width (W_3) on (a) S_{11} parameter and (b) axial ratio.

important parameter for the bandwidth of the axial ratio. Nevertheless, its influence on S_{11} is almost negligible.

4.2. The Influence of the Parameter W_3 on the Bandwidth and the Axial Ratio. The influence of the parameter W_3 on the reflection coefficient is not negligible, as shown in Figure 8. Although W_3 fluctuates between 6 mm and 10 mm, it does not significantly affect the bandwidth of the axial ratio. The impedance bandwidth is 3 GHz to 10 dB for $W_3 = 8$ mm.

4.3. The Influence of the Parameter W_2 on the Bandwidth and the Axial Ratio. The parameter W_2 is also an important constituent for the bandwidth of S_{11} and the axial ratio of the proposed geometry. The impedance bandwidth at 10 dB and

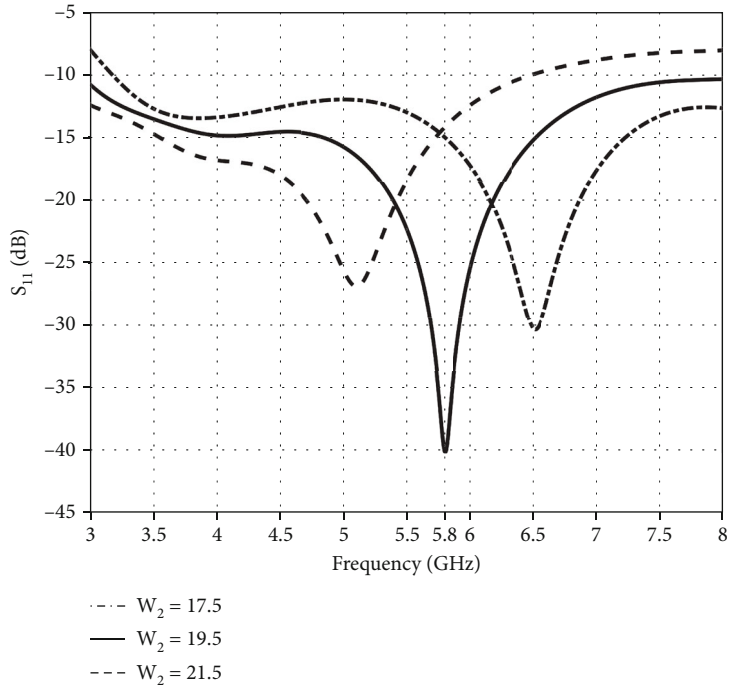

(a)

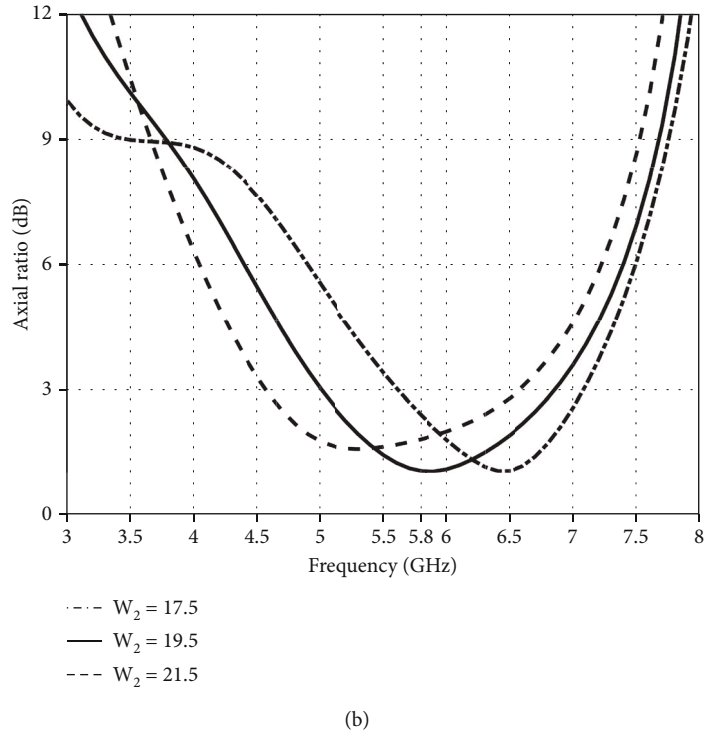

(b)

FIGURE 9: Influence of the width (W_2) on (a) S_{11} parameter and (b) axial ratio.

the axial ratio bandwidth at 3 dB are significant for W_2 = 19.5 mm, as shown in Figure 9.

4.4. The Influence of the Parameter W_9 on the Bandwidth and the Axial Ratio. Figure 10 illustrates precisely the influence of the parameter W_9 on the impedance bandwidth and axial ratio of the proposed antenna. The length of W_9 varies from 1 mm to 4 mm with an increment of 1.5 mm. The impedance bandwidth of 10 dB and the AR bandwidth of 3 dB are obtained for $W_9 = 2.5$ mm.

Thus, it can be concluded that the optimal parameters to achieve the desired objectives, namely, circular polarized ultrawideband and good S_{11} parameter matching, are W_2 = 19.5 mm, $W_3 = 8$ mm, $W_7 = 0.3$ mm, and $W_9 = 2.5$ mm. The simulation results confirm that the optimized rhombus ring antenna with slot has a good input impedance.

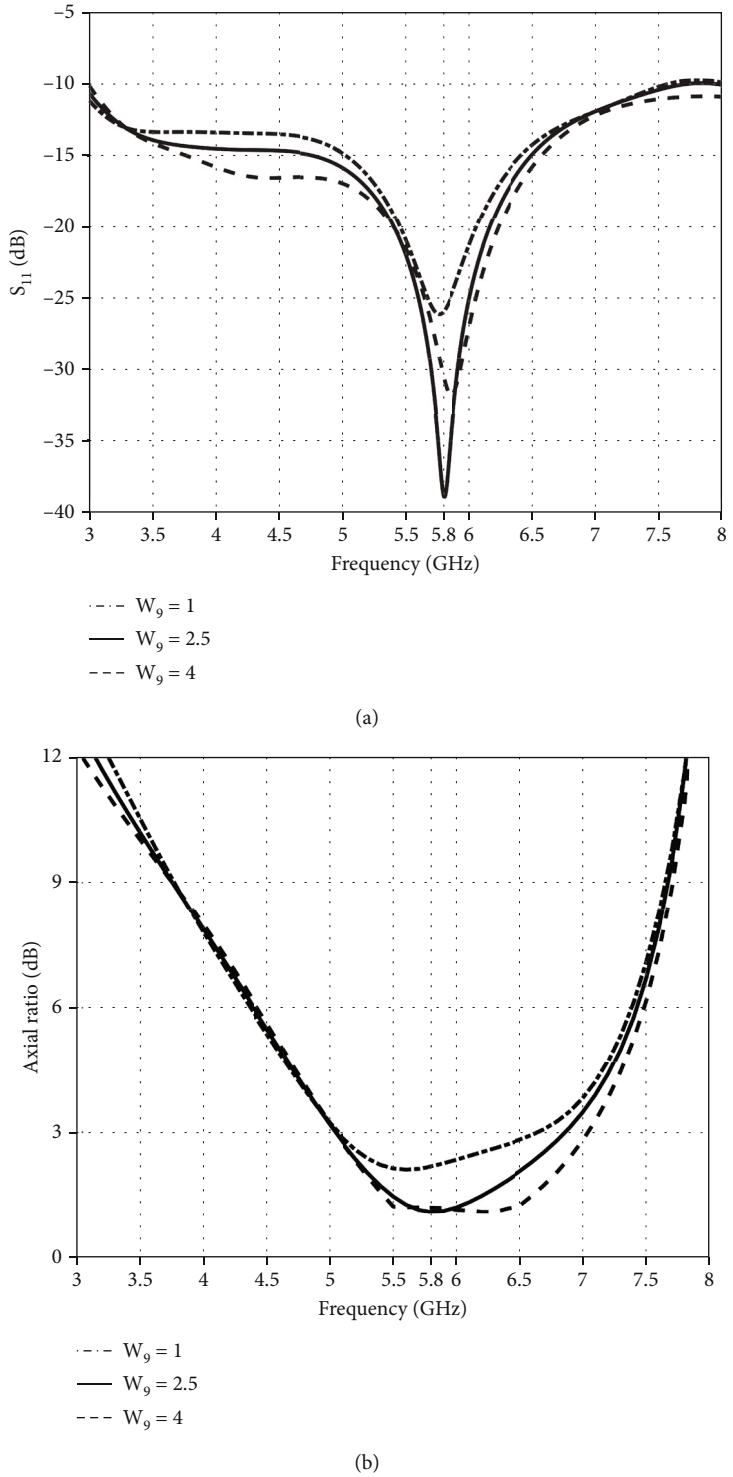

FIGURE 10: Influence of the width (W_9) on (a) S_{11} parameter and (b) axial ratio.

5. Input Impedance Calculation of the Conventional SRMSPA

In this section, the input impedance is calculated using the electromagnetic theory of the travelling wave transmission line developed in [26, 27]. In general, antenna design in microwave engineering is based on impedance control. Thus, for an antenna to radiate at the targeted working or excitation frequency, it must be perfectly matched to the lossless transmission line of length L of characteristic impedance Z_0, loaded by a terminal or antenna impedance Z_L (the load resistance Z_L is represented by the antenna). Several methods have been used in the literature such as those in [27–29]. We propose to determine the theoretical expression

of the impedance Z_{in} seen from the entrance of the line. From the theory of transmission lines, the input impedance of a transmission line is a function of the reflection coefficient by the relation

$$Z_{\text{in}}(z) = Z_0 \frac{1+\Gamma(z)}{1-\Gamma(z)}, \tag{1}$$

where $\Gamma(z) = \Gamma_L e^{-j2\beta z}$ is the input impedance of the line for a lossless substrate and is given by

$$Z_{\text{in}}(z) = Z_0 \frac{1+\Gamma_L e^{-j2\beta z}}{1-\Gamma_L e^{-j2\beta z}}, \tag{2}$$

where $\beta = \omega\sqrt{\mu\varepsilon}$ is the propagation constant.

The problem now is to find the charge reflection coefficient Γ_L. In reference [26], they considered the rectangular patch antenna as a parallel plate capacitor, and in this work, we will consider the square ring antenna as a parallel plate inductor of inductance.

$$L = \mu_0 h. \tag{3}$$

Next, let us find the relationship between the voltage and the current at the terminal of a parallel-plate inductor. We can write

$$V(z) = j\omega L I(z). \tag{4}$$

Putting $z = 0$, we have $V(0) = j\omega L I(0)$ or $Z_L = V(0)/I(0.)$. Thus, the load reflection coefficient is

$$\Gamma_L = \frac{j\omega\mu_0 h - Z_0}{j\omega\mu_0 h + Z_0}. \tag{5}$$

We assume hereafter that the antenna under study behaves as a transmission line of total length $L_2 + W_2$. Then, (5) will depend on the dimensions of the antenna, and the new expression for the input impedance of the square ring antenna is

$$Z_{\text{in}} = Z_0 \frac{1+\Gamma_L e^{-j2\beta(L_2+W_2)}}{1-\Gamma_L e^{-j2\beta(L_2+W_2)}}, \tag{6}$$

with $\Gamma_L = \Gamma_L(W_1) - \Gamma_L(W_2)$, $\Gamma_L(W_1) = j\omega\mu_0 h - Z_0(W_1)/j\omega\mu_0 h + Z_0(W_1)$, and $\Gamma_L(W_2) = j\omega\mu_0 h - Z_0(W_2)/j\omega\mu_0 h + Z_0(W_2)$.

6. Radiated Pattern Calculation

The radiated field is also calculated using a new approach based on the Biot and Savart law. In the analysis of antenna radiation problems, several methods have been used in other works such as the cavity model [26, 27] and that in [30, 31]. In our work, we will use Biot and Savart's law to calculate the radiated field at a long distance from the square ring antenna as rhombus or square ring gives the same results. This method consists first of all of calculating the magnetic induction created by a square ring, for which we will determine the expression of the current element vector. Then, the knowledge of magnetic induction will allow the calculation of the field radiated by the square ring antenna. Therefore, let us use Biot and Savart's law (which is a law of electromagnetism giving the magnetic induction $\vec{B}$ created by a DC current distribution) given by

$$\overrightarrow{dB} = \frac{\mu_0}{4\pi} \frac{\vec{dc} \wedge \overrightarrow{\text{PM}}}{\text{PM}^3}. \tag{7}$$

The antenna in general, and the square microstrip ring antenna in particular, is a radiation source that emits an

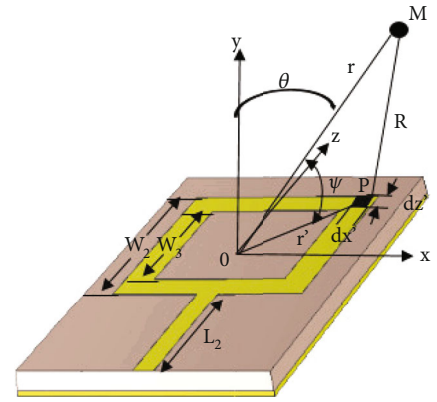

Figure 11: Coordinate systems of the fields radiated by a source placed at any position from the origin.

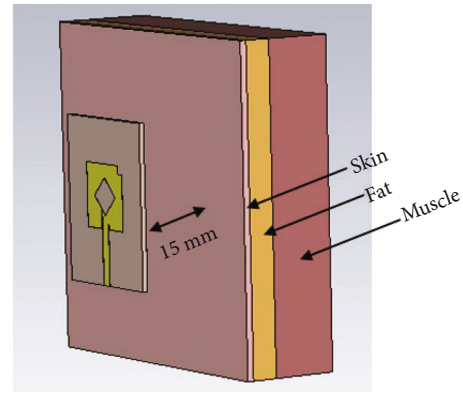

Figure 12: Rhombus ring antenna with human body pattern.

Table 3: Multilayered thickness specification.

Layer	Skin	Fat	Muscle
Thickness (in mm)	2	8	20

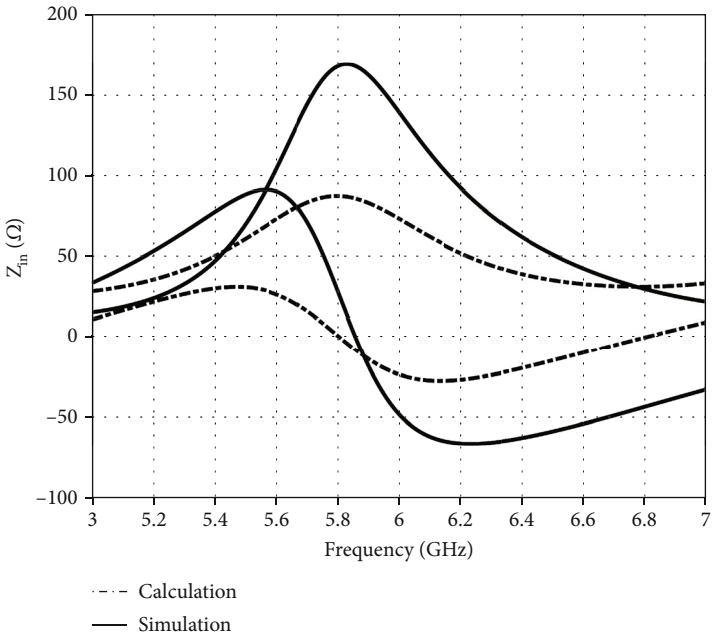

Figure 13: Input impedance of the square ring MSA obtained by calculation and simulation.

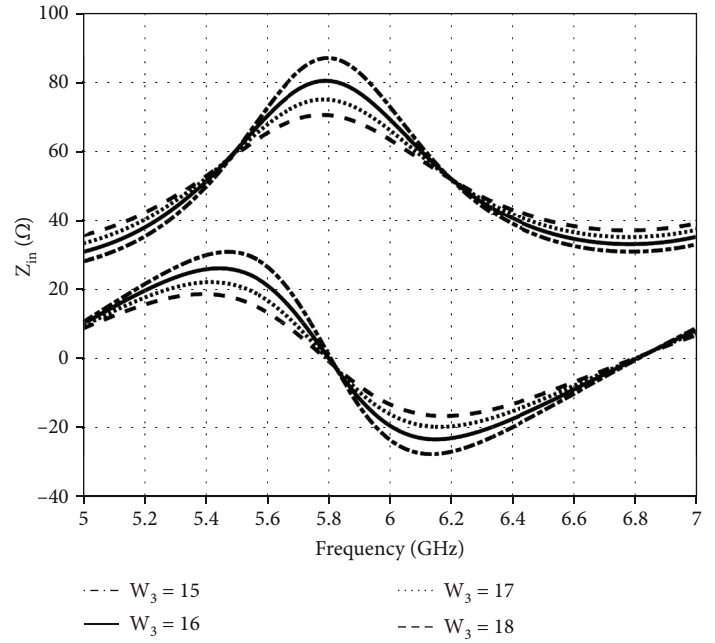

Figure 14: Effects of the inner ring on the input impedance of the square ring antenna.

electromagnetic wave for a given surface current distribution. We can then multiply relation (7) by $e^{-jk_0\mathrm{PM}}$. Thus

$$\overrightarrow{dB} = \frac{\mu_0}{4\pi}\frac{\vec{j}_s.ds\wedge\overrightarrow{\mathrm{PM}}}{\mathrm{PM}^3}e^{-jk_0\mathrm{PM}}. \quad (8)$$

We will now consider the antenna as a parallel plate waveguide formed by two conductive plates. The expression for the surface current density vector has been established in reference [32]. Thus

$$\vec{j}_s = \frac{V_0}{\eta h}e^{-j\beta z'}\vec{e}_z. \quad (9)$$

Then, the expression of the elementary magnetic induction vector is as follows:

$$\overrightarrow{dB} = \frac{\mu_0}{4\pi}\frac{V_0}{\eta h}\frac{e^{-j\beta z'}.ds\vec{e}_z\wedge\overrightarrow{\mathrm{PM}}}{\mathrm{PM}^3}e^{-jk_0 r}f(\theta,\phi), \quad (10)$$

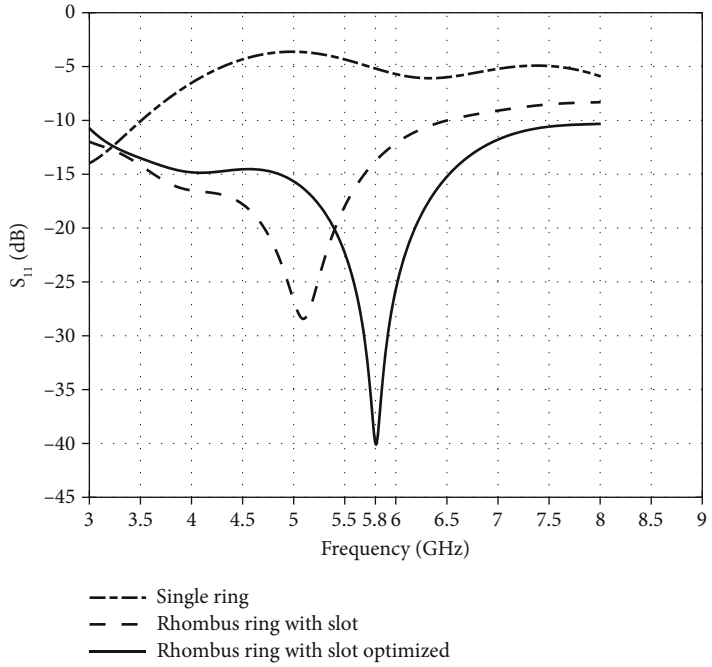

FIGURE 15: S_{11} parameter of the different geometries.

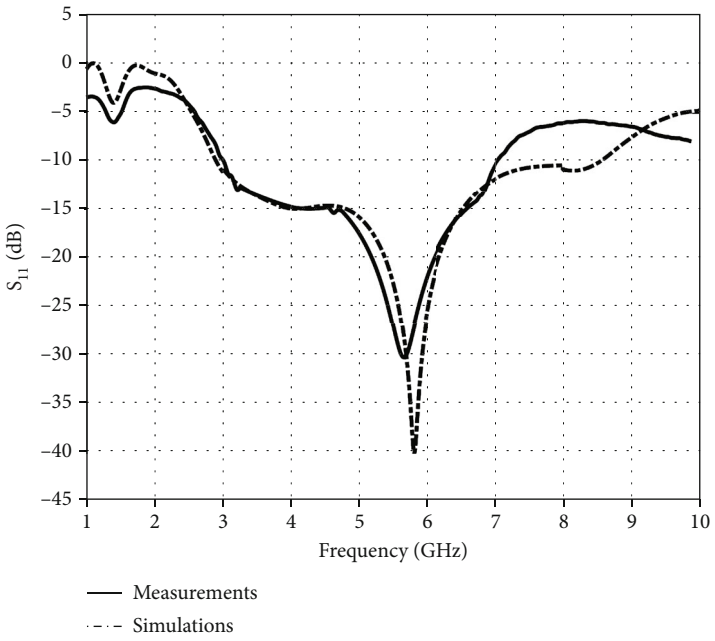

FIGURE 16: Simulated and measured S_{11} parameter.

with $f(\theta, \phi) = e^{jk_0(x' \sin\theta \cos\phi + z' \cos\theta)}$

We therefore express the vector product appearing in Biot and Savart's law as depicted in the next equation.

$$e^{-j\beta z'} . ds \vec{e}_z \wedge \overrightarrow{\mathrm{PM}} = \begin{pmatrix} -r dx' dz' e^{-j\beta z'} \sin\theta \sin\phi \\ r dx' dz' e^{-j\beta z'} \sin\theta \cos\phi \\ 0 \end{pmatrix}. \quad (11)$$

Substituting relation (11) into (10), we have the expression of the magnetic induction vector according to the square ring (see Figure 11).

$$\vec{B} = \begin{pmatrix} -f_1 \sin\phi \iint_{W_3/2}^{W_2/2} dx' dz' e^{jk_z z'} e^{jk_x x'} \\ f_1 \cos\phi \iint_{W_3/2}^{W_2/2} dx' dz' e^{jk_z z'} e^{jk_x x'} \\ 0 \end{pmatrix}, \quad (12)$$

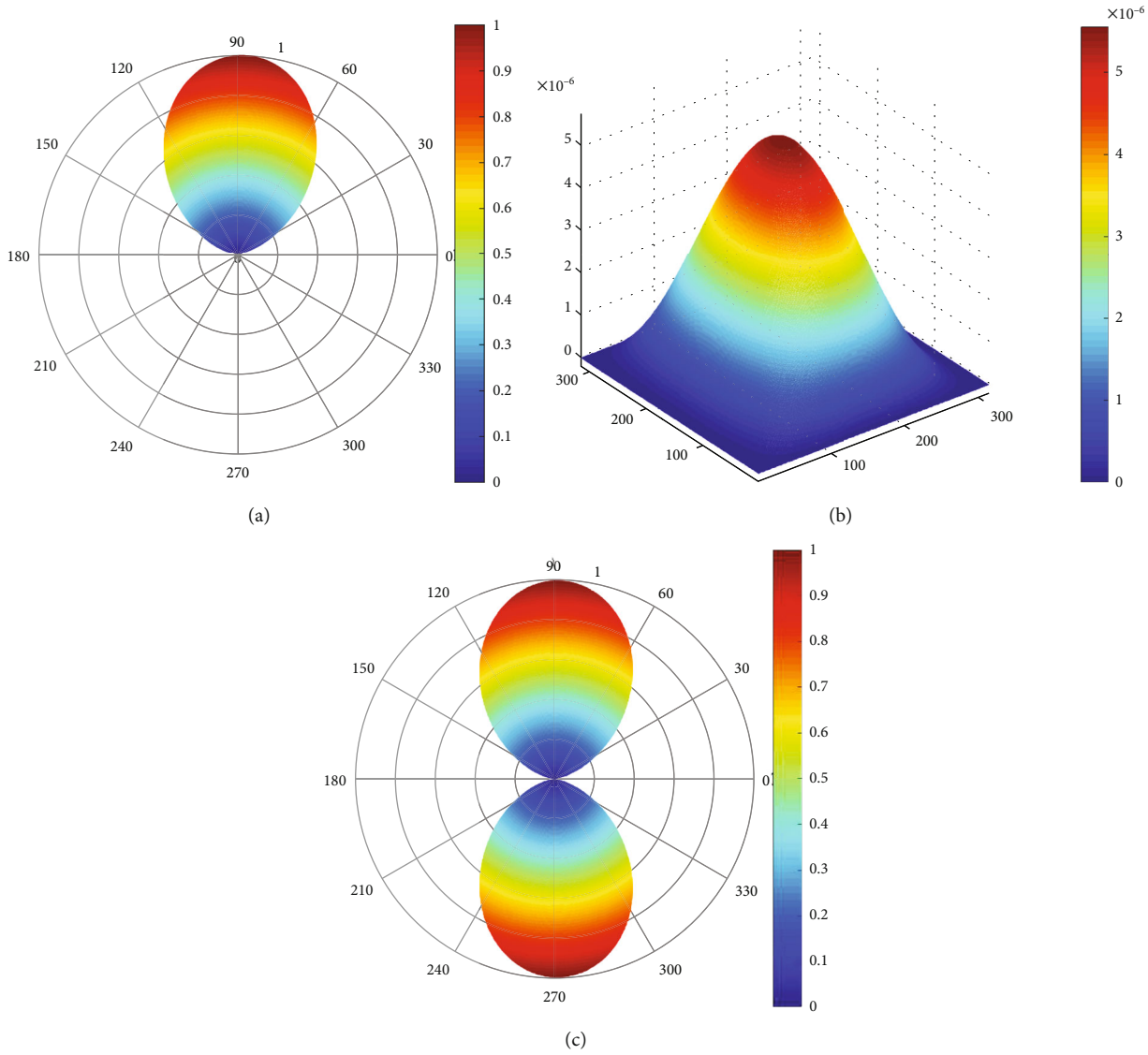

Figure 17: Calculated radiation pattern. (a) Polar 2D SRMSPA, (b) Cartesian 3D SRMSPA, and (c) polar 2D RRMSMA.

with $f_1 = V_0\mu_0/4\pi\eta h \sin\theta/r^2 e^{-jk_0 r}$, $k_x = k_0 \sin\theta\cos\phi$, and $k_z = k_0\cos\theta - \beta$.

Thus, the expressions of the electric field components with the array factor in a square-ring microstrip antenna are

$$E_\theta(\theta,\phi) = jQR(\theta,\phi)\sin(k_0 h\sin\theta\sin\phi)\sin\theta, \quad E_\phi = 0 \tag{13}$$

With $R(\theta,\phi) = (e^{jk_x W_3/2} - e^{jk_x W_2/2})(e^{jk_z W_2/2} - e^{jk_z W_3/2})/k_x k_z$, $k_x = k_0\sin\theta\cos\phi$, $k_z = k_0\cos\theta - \beta$, $Q = V_0/4\pi h e^{-jk_0 r}$, and $\beta = \omega\sqrt{\mu_0\varepsilon}$.

7. Numerical Behavior of the Proposed Antenna on a Part of the Phantom Model

To evaluate the SAR value of the human body cell, a part of the phantom model of size $100 \times 100 \times 30\,\text{mm}^3$ was developed using CST-MWS. As shown in Figure 12, skin, fat, and muscle layers are considered to model on a part of the phantom model. Bone is not included in the simulation as it does not affect the results due to its depth and only increases the computational complexity and therefore the simulation time. Table 3 shows the thickness of each layer for building the layered structure.

8. Results and Discussion

Input and output performances of the proposed antenna etched on the Rogers (RO4003) dielectric substrate of relative permittivity $\varepsilon_r = 3.55$, thickness $h = 1.524\,\text{mm}$, and loss tangent $\tan\delta = 0.0027$ are reported. The numerical behavior of the studied radiator on a part of the phantom is then considered.

To validate the proposed antenna, input impedance calculation method result values obtained are compared to the simulation, and the results are depicted in Figure 13. It can

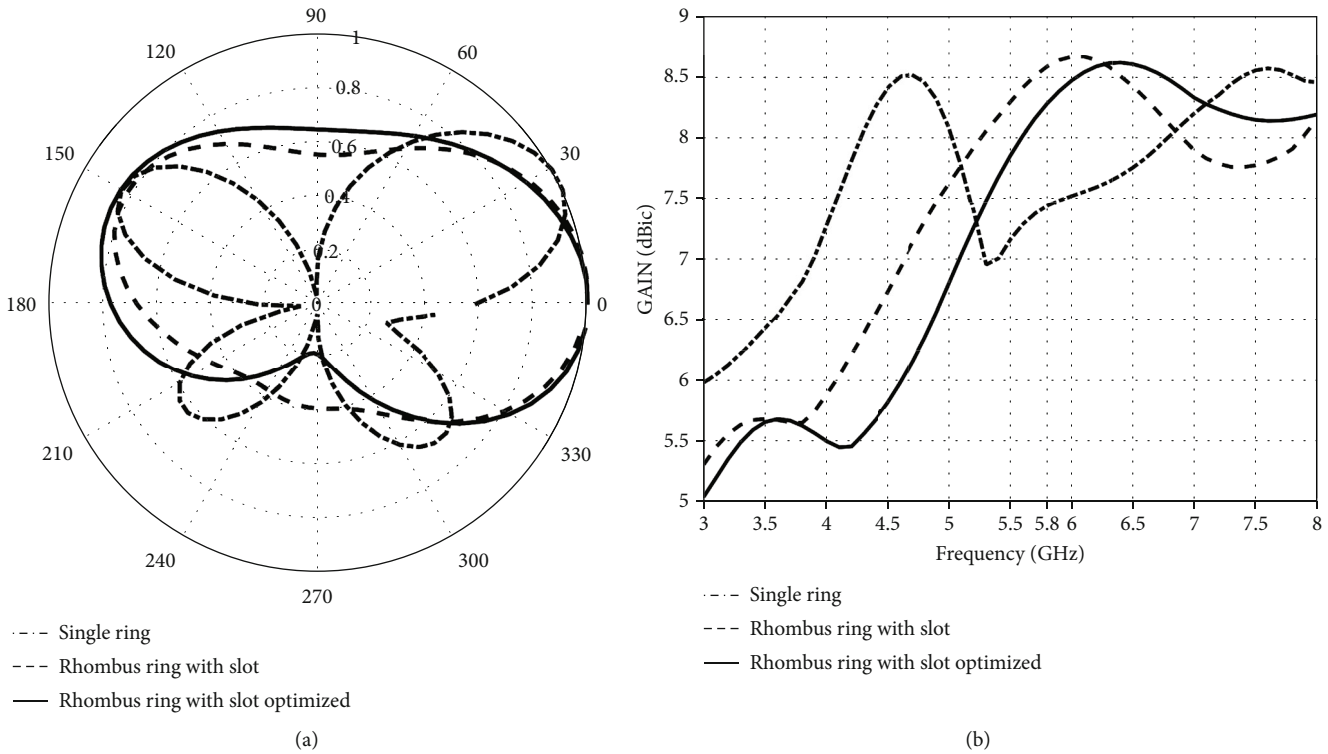

Figure 18: Simulation of radiation characteristics. (a) Electric field pattern and (b) gain.

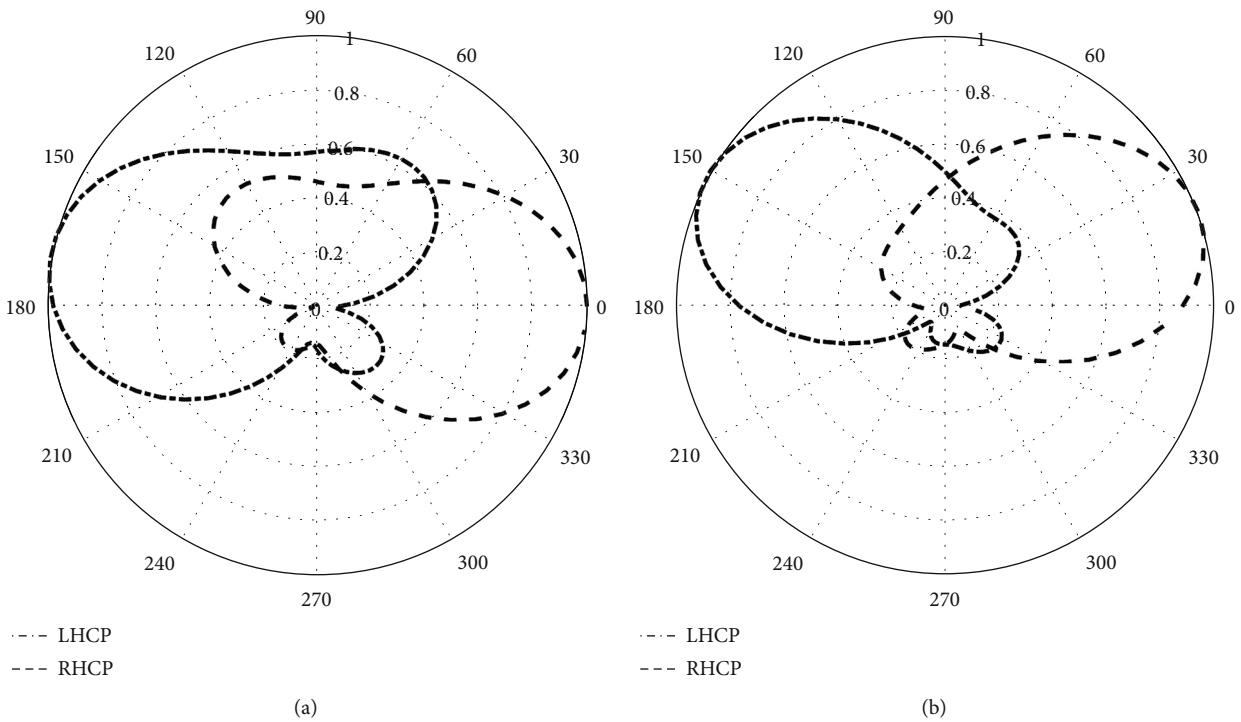

Figure 19: Normalized LHCP and RHCP pattern at 5.8 GHz (a) E-plane and (b) H-plane.

be seen that these curves are identical, although there is a slight shift of the frequency to the right and a difference in the input resistance is due to the accuracy of the proposed calculation method.

Figure 14 shows the effects of the inner ring on the input impedance of the square ring microstrip patch antenna as a function of frequency. We can see that as the dimensions of the inner ring increase, the input resistance decreases, so the

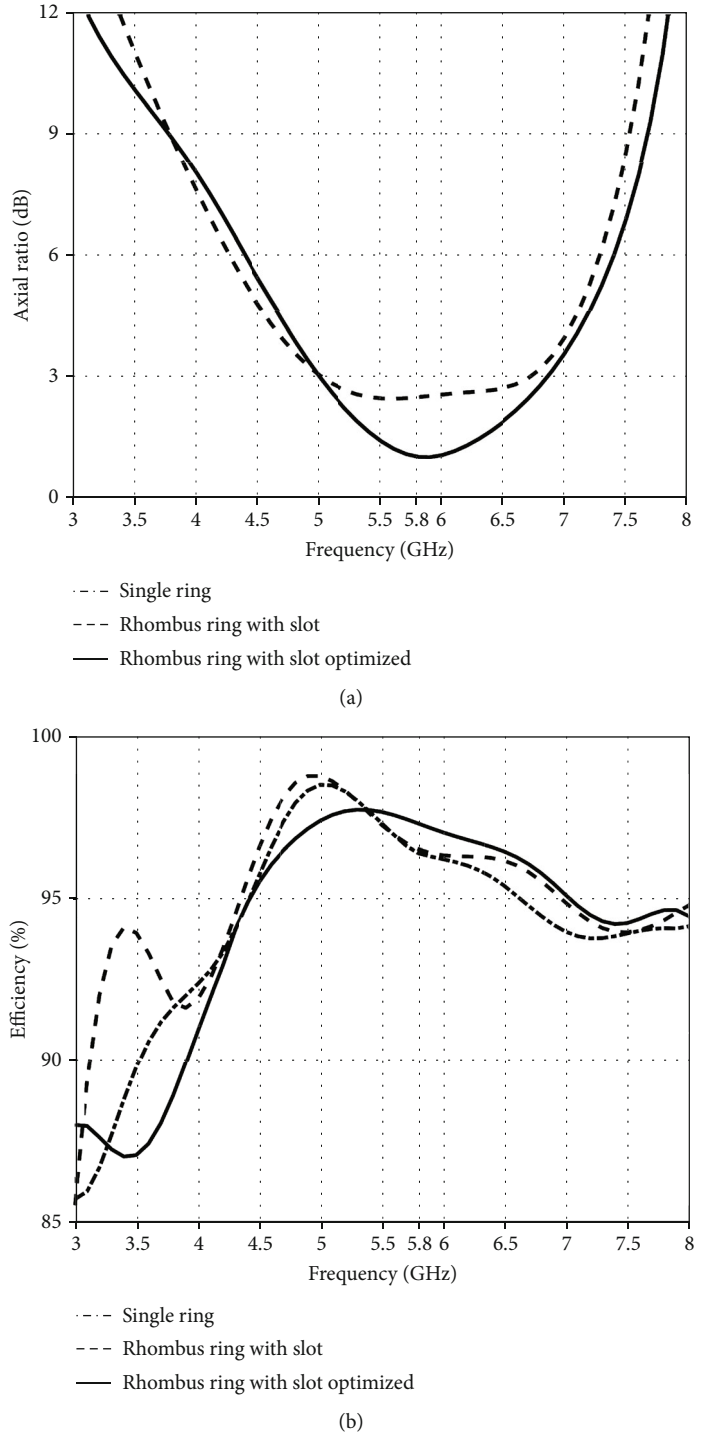

Figure 20: (a) Axial ratio and (b) efficiencies of different geometries.

antenna behaves as a slightly resistive circuit. Therefore, this increase in dimensions will allow us to obtain an input resistance of 50 Ω which will prove the matching between the feed line and the antenna.

The simulated input performance of different geometries of the studied antenna is shown in Figure 15. It can be clearly seen that the proposed rhombus ring MSA circular polarized exhibits good impedance matching corresponding to an input resistance of 45 Ω with a minimum S_{11} parameter of about -40 dB, a wider bandwidth of -10 dB impedance bandwidth of around 86.20% (3-8 GHz) centered at the frequency of 5.8 GHz.

Figure 16 shows simulated and measured results. We can observe that all curves are identical. Nevertheless, experimental results show that the proposed antenna exhibits a -10 dB impedance bandwidth of about 3-7 GHz centered at the frequency of 5.8 GHz with a minimum S_{11} parameter of -32 dB. The slight differences observed can be explained

Table 4: Comparison between the proposed antenna and other references.

References	Frequency (GHz)	Dimension (mm^3)	Impedance bandwidth (%)	Polarization	Peak gain
[17]	4.74	$20 \times 20 \times 1.5$	36.9	CP	3.0 dBic
[21]	2.48 and 3.16	$35 \times 30 \times 1.6$	6.04 and 1.94	CP, LP	1.05 and 1.09 dB
[33]	—	$65.5 \times 42.4 \times 1.6$	20.9	CP	7 dB
[34]	—	$25 \times 25 \times 0.80$	52	CP	3.6 dB
This work	5.8	$19.5 \times 19.5 \times 1.524$	86.20	CP	8.29 dBic

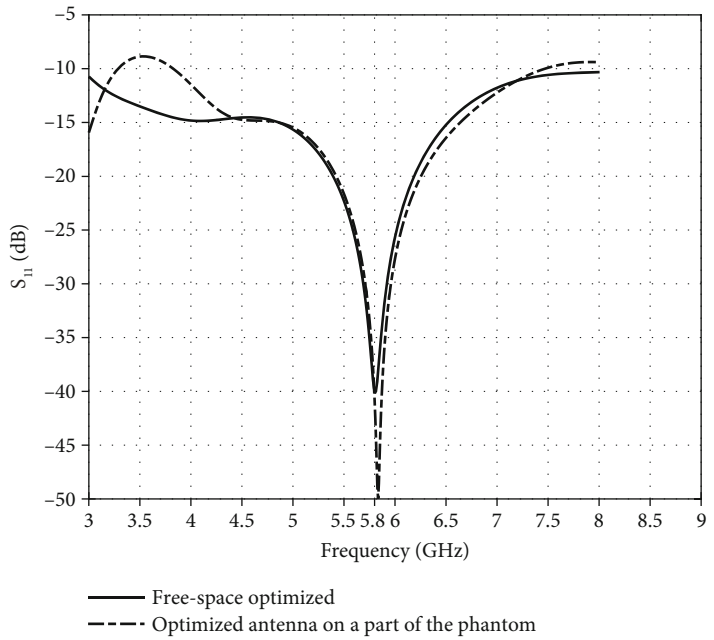

Figure 21: The behavior of the S_{11} parameter of the proposed antenna on a part of the phantom and in free space.

by the condition of fabrication and measurement and the connection between the microstrip feed line and SMA connector with the measurement of the environment that simulations do not take into account.

The calculated electric field radiation pattern in the θ-direction in linear scale at the working frequency of 5.8 GHz is illustrated in Figure 17. We can observe that the proposed antenna radiates as the conventional MSPA with a unidirectional radiation pattern perpendicular to the antenna plane (Figure 17(b)) and exhibits a -3 dB beamwidth of about 90° (Figure 17(a)). This result is in good agreement with the result proposed in [26].

Figure 18 illustrates simulated radiation characteristics of different geometries of the studied antenna at the working frequency of 5.8 GHz. We can establish that the optimized slotted rhombus ring MSA has a quasi-omnidirectional radiation pattern due to the presence of the DGS. However, all the investigated geometries radiate on all the studied bandwidths (3-8 GHz), and the maximum stable gain obtained near the working frequency is around 8.8 dBic. The simulated E-plane and H-plane radiation pattern in Figure 19 affirm the dominance of right-hand circular polarization (RHCP) over left-hand circular polarization (LHCP) at 5.8 GHz.

Figure 20(a) depicts simulated results of the axial ratio of different geometries of the studied antenna. It appears that the optimized slotted rhombus ring MSA exhibits circular polarization and a 3 dB bandwidth of 32.75%, and an axial ratio of around 1.04 dB has been obtained. The passband efficiency of the proposed antenna is about 97.7% at the working frequency of 5.8 GHz, as shown in Figure 20(b). A comparative summary performance of the proposed antenna with some other references is conferred in Table 4. In comparison with some other published works, the proposed design is simple and attractive. It achieves in more circular polarization better performances such as low volume, wide bandwidth, and acceptable real stable gain.

Figure 21 reports simulated input characteristics of the studied antenna on a part of the phantom and in free space. It can be clearly seen that all the curves are identical and input performances are preserved. Hence, the on-body optimized slotted rhombus ring MSA proposed has negligible effects on the input performances of the antenna.

Numerical radiation performances of the circularly polarized slotted rhombus ring MSA on a part of the phantom are shown in Figure 22. It is noted that the stable maximum gain of about 9.64 dB is obtained, and the observation of the obtained radiation pattern shows that the human

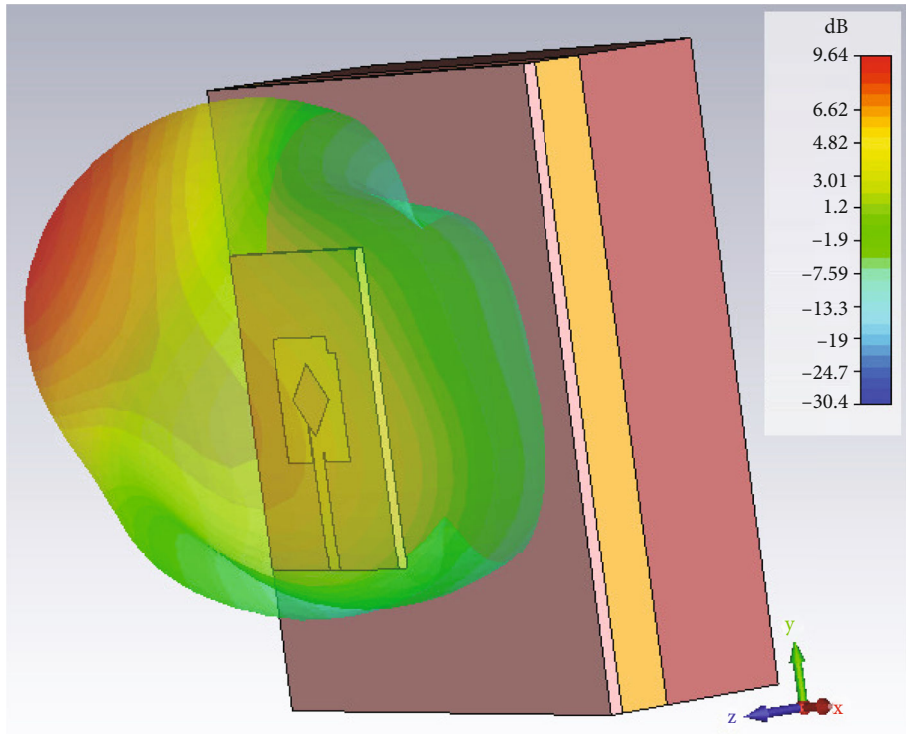

(a)

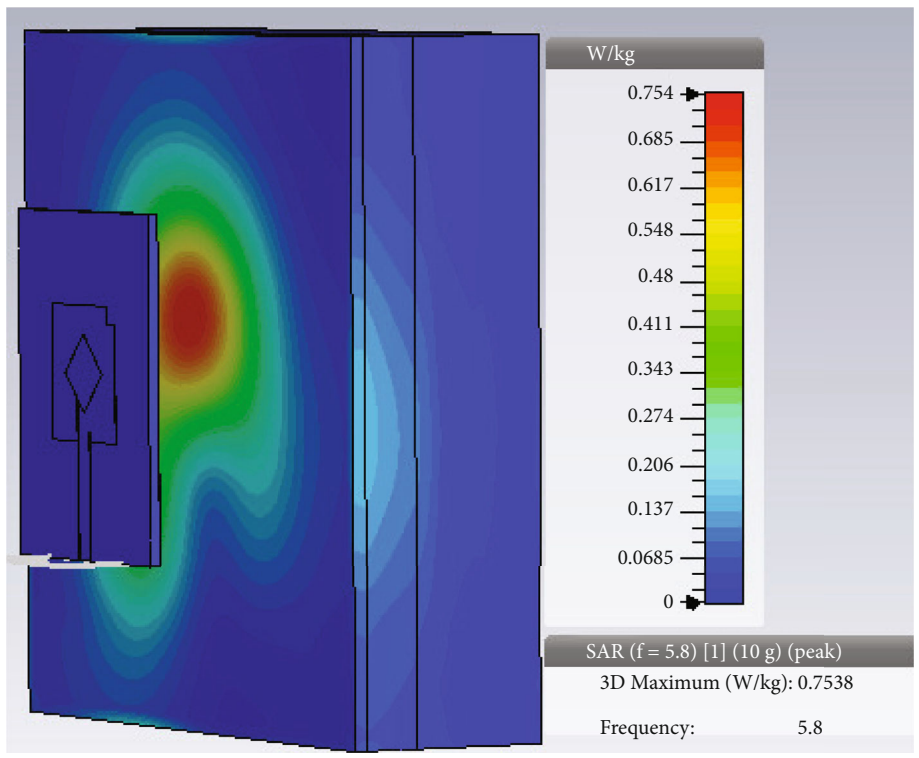

(b)

Figure 22: Radiation characteristics at 5.8 GHz of the antenna studied in part of the phantom. (a) Gain and (b) specific absorption rate.

body is well protected from the exposure of the antenna radiation, as illustrated in Figure 22(a). Assuming an input power of 1 w, the maximum SAR values obtained are around 1.45 and 0.754 W/Kg on 1 and 10 g of tissue mass, respectively, at 5.8 GHz, as shown in Figure 22(b). These values are following the prescriptions of IEC and FCC that make the studied antenna as a serious candidate for WBAN applications. As experimental perspective work, measurements

concerning radiation patterns and SAR characteristics will be done in real conditions.

9. Conclusions

On-body rhombus ring microstrip monopole antenna exhibiting circular polarization for WBAN applications has been investigated. Circular polarization performance was achieved by cutting a part of metallization at one side of the notch near the feed line of the studied SRRMSMA. One vertex of the proposed radiating element was truncated for bandwidth broadening. The proposed SRRMSMA exhibits an UWB behavior so that -10 dB impedance bandwidth achieved of relative bandwidth is about 86.20% in the 3-8 GHz frequency band. A significant AR bandwidth of 3 dB (32.75%) with a high peak gain of 8.29 dBic and a radiation efficiency of over 95% was obtained. SAR analysis using a three-layer human phantom model is also performed to validate the possible use of the proposed antenna in the telemedicine application with the goal of transmitting patient parameters in real-time with minimum losses towards a remote service centre for rapid patient care. It is observed that the maximum amount of radiation absorbed by the body model is limited to a maximum SAR value of 1.45 W/kg and 0.754 W/kg for 1 g and 10 g of tissue mass, respectively. Based on the achieved performance, the designed SRRMSMA revealed a promoter interest for the future such as compactness and wide bandwidth covering the whole band of 3-7 GHz. Hence, the studied antenna is a good candidate for present and future wireless communications systems such as WLAN in 5G sub-6 GHz, FR1 6G band, and WBAN for good patient care in the context of far-medicine.

Data Availability

The data that support the findings of this study are available on request from the corresponding author. The data are not publicly available due to privacy or ethical restrictions.

Conflicts of Interest

The authors declare that they have no conflicts of interest.

References

[1] D. M. Barakah, "A survey of challenges and applications of wireless body area network (WBAN) and role of a virtual doctor server in existing architecture," in *2012 Third International Conference on Intelligent Systems Modelling and Simulation*, pp. 214–219, Kota Kinabalu, Malaysia, 2012.

[2] B. Zhen, H. B. Li, and R. Kohno, "Networking issues in medical implant communications," *International Journal of Multimedia and Ubiquitous Engineering*, vol. 4, no. 1, pp. 23–37, 2009.

[3] G. K. Ragesh and K. Baskaran, "An overview of application, standards and challenges in futuristic wireless body area networks," *International Journal of Computer Science Issues*, vol. 9, no. 2, pp. 180–186, 2012.

[4] P. S. Hall and Y. Hao, *Antenna and Propagation for Body-Centric Wireless Communications*, Artech House, Norwood, 2012.

[5] Y. Coulibaly, M. Nedil, L. Talbi, and T. A. Denidni, "High gain cylindrical dielectric resonator with superstrate for broadband millimeter-wave underground mining communications," in *2010 14th International Symposium on Antenna Technology and Applied Electromagnetics & the American Electromagnetics Conference*, Ottawa, ON, Canada, 2010.

[6] M. N. Suma, P. C. Bybi, and P. Mohanan, "A wideband printed monopole antenna for 2.4-GHz WLAN applications," *Microwave and Optical Technology Letters*, vol. 48, no. 5, pp. 871–873, 2006.

[7] P. J. Soh, G. A. E. Vandenbosch, S. L. Ooi, and N. H. M. Rais, "Design of a broadband all-textile slotted PIFA," *IEEE Transactions on Antennas and Propagation*, vol. 60, no. 1, pp. 379–384, 2012.

[8] A. Alomainy, Y. Hao, A. Owadally et al., "Statistical analysis and performance evaluation for on-body radio propagation with microstrip patch antennas," *IEEE Transactions on Antennas and Propagation*, vol. 55, no. 1, pp. 245–248, 2007.

[9] N. Haga, K. Saito, M. Takahashi, and K. Ito, "Characteristics of cavity slot antenna for body-area networks," *IEEE Transactions on Antennas and Propagation*, vol. 57, no. 4, pp. 837–843, 2009.

[10] R. Moro, S. Agneessens, H. Rogier, and M. Bozzi, "Wearable textile antenna in substrate integrated waveguide technology," *Electronics Letters*, vol. 48, no. 16, pp. 985–987, 2012.

[11] A. Zeghdoud, M. C. Derbal, and M. Nedil, "Gain optimisation of a YagiUda antenna using the genetic algorithm," in *2019 IEEE International Symposium on Antennas and Propagation and USNC-URSI Radio Science Meeting*, pp. 1041-1042, Atlanta, GA, USA, 2019.

[12] A. Habani, M. Nedil, M. Elazhari, and F. Ghanem, "High gain off-body antenna based on the combination AMC-FSS structure for underground mining communications," in *2016 IEEE International Symposium on Antennas and Propagation (APSURSI)*, pp. 267-268, Fajardo, PR, USA, 2016.

[13] A. Zeghdoud and M. Nedil, "Off-body dipole antenna with dogbone-shaped AMC bending on the human arm," in *2019 IEEE International Symposium on Antennas and Propagation and USNC-URSI Radio Science Meeting*, pp. 1115-1116, Atlanta, GA, USA, 2019.

[14] M. S. H. Mollah, O. Faruk, M. S. Hossain, M. T. Islam, A. S. M. Shafi, and M. M. I. Molla, "Design and performance improvement of microstrip patch antenna using graphene material for communication applications," in *2021 IEEE 11th IEEE Symposium on Computer Applications & Industrial Electronics (ISCAIE)*, pp. 343–346, Penang, Malaysia, 2021.

[15] V. Sharma, M. D. Upadhayay, A. V. Singh, and J. Prajapati, "Hammer-shaped element-based compact MIMO antenna for WLAN application," *Progress In Electromagnetics Research Letters*, vol. 97, pp. 121–130, 2021.

[16] A. Kayabasi, "Triangular ring patch antenna analysis: neuro-fuzzy model for estimating of the operating frequency," *Aces Journal*, vol. 36, no. 11, pp. 1412–1417, 2021.

[17] S. Patil, A. Verma, A. K. Singh, B. K. Kanaujia, and S. Kumar, "A lowprofile circularly polarized microstrip antenna using elliptical electromagnetic band gap structure," *International Journal of Microwave and Wireless Technologies*, vol. 14, no. 8, pp. 1009–1018, 2021.

[18] Z. L. Ma and C. W. Zhang, "3-D printed circularly polarized open-ended waveguide antenna array based on an in-built antipodal exponential groove polarizer," *International Journal of RF and Microwave Computer-Aided Engineering*, vol. 2023, Article ID 4824224, 9 pages, 2023.

[19] J. K. Liu, X. L. Zha, C. X. Zhang, and Z. Y. Wang, "A novel low axis ratio double-circularly polarized microstrip antenna," *International Journal of Antennas and Propagation*, vol. 2022, Article ID 8947697, 7 pages, 2022.

[20] G. Singh, B. K. Kanaujia, V. K. Pandey, and S. Kumar, "Quad-band multi-polarized antenna with modified electric-inductive −capacitive resonator," *International Journal of Microwave and Wireless Technologies*, vol. 14, no. 1, pp. 65–76, 2022.

[21] G. Singh, B. K. Kanaujia, V. K. Pandey, D. Gangwar, and S. Kumar, "Design of compact dual-band patch antenna loaded with D-shaped complementary split ring resonator," *Journal of Electromagnetic Waves and Applications*, vol. 33, no. 16, pp. 2096–2111, 2019.

[22] T. N. Cao, M. T. Nguyen, H. L. Phan et al., "Millimeter-wave broadband MIMO antenna using metasurfaces for 5G cellular networks," *International Journal of RF and Microwave Computer-Aided Engineering*, vol. 2023, Article ID 9938824, 11 pages, 2023.

[23] F. M. Alnahwi, Y. I. A. Al-Yasir, C. H. See, and R. A. Abd-Alhameed, "Single-element and MIMO circularly polarized microstrip antennas with negligible Back radiation for 5G mid-band handsets," *Sensors*, vol. 22, no. 3067, pp. 1–13, 2022.

[24] Q. Wu, Y. Shi, and L. Li, "Wideband dual-polarized differential-fed filtering microstrip patch antenna with high suppression and wide stopband," *International Journal of RF and Microwave Computer-Aided Engineering*, vol. 2023, Article ID 6682038, 10 pages, 2023.

[25] S. Das, H. Islam, T. Bose, and N. Gupta, "Ultra wide band CPW-fed circularly polarized microstrip antenna for wearable applications," *Wireless Personal Communications*, vol. 108, no. 1, pp. 87–106, 2019.

[26] C. Mbinack, "Dual-band microstrip-fed SQUARE ring antenna input and output performances analysis for Wi-Fi application," *Microwave and Optical Technology Letters*, vol. 61, no. 4, pp. 1011–1015, 2019.

[27] C. Mbinack, E. Tonye, and D. Bajon, "Microstrip-line theory and experimental study for the characterization of the inset-fed rectangular microstrip-patch antenna impedance," *Microwave and Optical Technology Letters*, vol. 57, no. 2, pp. 514–518, 2015.

[28] M. A. Karim, S. Naoui, L. Latrach, and A. Gharsallah, "Design of a compact size tag antenna based on a split ring resonator for UHF RFID application," *International Journal of RF and Microwave Computer-Aided Engineering*, vol. 29, no. 7, Article ID e21607, 2018.

[29] V. G. Kasabegoudar, "Analysis of coplanar capacitive coupled wideband microstrip antennas," *International Journal of Engineering Trends and Technology*, vol. 69, no. 9, pp. 45–50, 2021.

[30] S. Sharma, C. C. Tripathi, and R. Rishi, "Impedance matching techniques for microstrip patch antenna," *Indian Journal of Science and Technology*, vol. 10, no. 28, pp. 1–16, 2017.

[31] H. M. Bernety, "Analytical phasing of arbitrarily oriented arrays using a fast, analytical far-field calculation method," *IEEE Transactions on Antennas and Propagation*, vol. 66, no. 6, pp. 1558–2221, 2018.

[32] D. M. Pozar, *Microwave Engineering*, John Wiley & Sons, 3rd edition, 2005.

[33] T. Miyazaki, J. T. S. Sumantyo, A. Takahashi, and M. Naito, "Development of circularly polarized microstrip antenna for high temperature environment observation by synthetic aperture radar," in *2021 7th Asia-Pacific Conference on Synthetic Aperture Radar (APSAR)*, Bali, Indonesia, 2021.

[34] V. Rafi, J. Nourinia, C. Ghobadi, J. Pourahmadazar, and B. S. Virdee, "Broadband circularly polarized slot antenna array using sequentially rotated technique for C-band applications," *IEEE Antennas and Wireless Propagation Letters*, vol. 12, pp. 128–131, 2013.